MATEC Web of Conferences **33**, 05005 (2015)
DOI: 10.1051/matecconf/20153305005

Compositional trends in Ni-Mn-Ga Heusler alloys: first-principles approach

Vladimir Sokolovskiy[1a], Yulia Sokolovskaya[1], Vasiliy D. Buchelnikov[1], M. Zagrebin[1] and Alexey T. Zayak[2]

[1]*Chelyabinsk State University, Condensed Matter Department, 454001 Chelyabinsk, Russia*
[2]*Bowling Green State University, Department of Physics and Astronomy, OH-43403 Bowling Green, USA*

Abstract. In this work we present a systematic investigation of magnetic and structural properties of a broad range of Ni-Mn-Ga alloys by means of the density functional theory. Calculations are carried out for the cubic austenitic phase. The effect of chemical disorder is simulated by using the single-site coherent-potential approximation and the spin-polarized generalized gradient approximation. Equilibrium lattice parameters, bulk moduli, total magnetic moments, and formation energies of a wide range of Heusler alloys have been mapped on compositional ternary diagrams that give a bigger picture of the variety of physical properties of this family of alloys.

1 Introduction

Heusler alloys are ternary or quaternary intermetallic compounds known for several technologically promising features, for example, the magneto-structural coupling that yields the so-called magnetic shape-memory effect or giant magnetocaloric effect. Ternary Heusler alloys are typically known to be magnetic and assume a cubic ($L2_1$ or B_2) crystal structure with a generic chemical formula X_2YZ (where B_2 is like the $L2_1$ structure, but with some disorder on the Y and Z sites) [1, 2]. The X and Y sites are typically occupied by transition 3*d* metal elements, while the Z site contains some *sp* elements, like Ga, Ge.

At present, among many ferromagnetic (FM) shape memory alloys, Ni-Mn-Ga Heusler systems are the most studied by means of theoretical and experimental approaches (for example, see Refs. [1-15]). Such high interest is related to the unique properties exhibited by the prototypical stoichiometric shape-memory compound Ni_2MnGa. However, while the stoichiometric compound is the canonical Heusler system, the richness of its properties can be significantly extended with many chemical substitutions. A variety of different off-stoichiometric Ni-Mn-Ga compositions, which have been synthesized and characterised in past twenty years are mappen on the ternary diagram shown in Fig. 1. Here, we have collected about 900 compositions of Ni-Mn-Ga, but this summary is far from being complete. This diagram clearly indicates that the most popular compositions are localized are localized in the middle part of a ternary diagram, close to the stoichiometric system. The majority of well-studied compounds belong to the families of $Ni_{2+x}Mn_{1-x}Ga$ (x = 0.0 – 0.39) and $Ni_2Mn_{1+x}Ga_{1-x}$ (x = 0.0 – 0.4), showing a strong coupling between the magnetic and structural subsystems [10]. But overall, on the bigger picture we see that a large area on the compositional diagram of Ni-Mn-Ga remains to be explored, but it may potentially lead to discoveries for important functional properties.

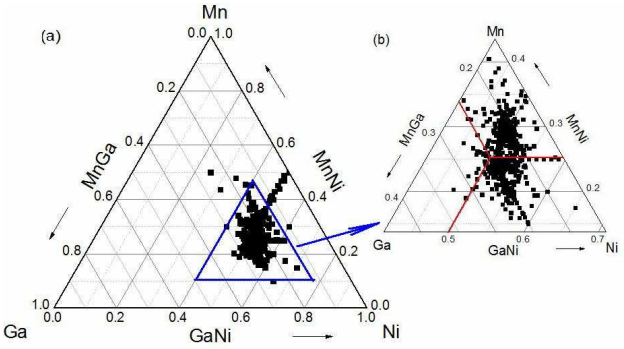

Figure 1. Compositional ternary phase diagram of Ni-Mn-Ga compounds. The points map the most studied compositions reported in the literature.

We would like to emphasize that computational approaches on the level of the density functional theory (DFT) have been quite successful in describing electronic, structural, magnetic and dynamical properties of Ni-Mn-Ga Heusler alloys [10]. However, it is important to recognize that the theoretical studies of Heusler alloys are traditionally limited to stoichiometric compositions such as Ni_2MnGa. The reason for that is the natural difficulty of a theoretical description of a random system, while some computational approaches have achieved substantial success in studies of off-stoichiometric systems. This task remains very challenging. There is no "perfect" theoretical tool that would provide comprehensive descriptions of an off-stoichiometric system, like the family of Ni-Mn-Ga

[a] Corresponding author: vsokolovsky84@mail.ru

Article available at http://www.matec-conferences.org or http://dx.doi.org/10.1051/matecconf/20153305005

compounds. On the other hand, experimental studies mainly deal with wide ranges of chemical compositions. This gap between the experimental situation and the theoretical picture needs to be closed by the computational research.

In this work we perform a wide-range systematic study of the family off-stoichiometric Ni-Mn-Ga alloys by using the coherent potential approximation (CPA) in the framework of DFT. Our goal is explore the compositional variations of the structural stability and magnetic properties of Ni-Mn-Ga compositions, especially focusing on the areas that have not been covered by the experimental research.

2 *Ab initio* calculation details

In order to simulate the range of chemical compositions of Ni-Mn-Ga alloy, we employ the spin-polarized relativistic Korringa-Kohn-Rostoker (SPR-KKR) electronic structure code [16]. It is based on the density functional theory and uses the generalized gradient approximation for the exchange correlation functional in the formulation of Perdew, Burke and Ernzerhof (PBE) [17]. Calculations of equilibrium lattice parameters, bulk moduli, and total magnetic moments were carried out for austenitic $L2_1$ structure (space group $Fm\underline{3}m$). The chemical disorder was simulated by using the single-site coherent-potential approximation (CPA), which is designed specifically to describe disordered systems by composing weighted fractions of various chemical species. This approach implies that on a specific atomic site one can have a virtual atom that is composed of X% of atomic species A and (100-X)% of atomic species B, thus allowing for simulations with wide ranges of off-stoichiometric compositions within a normal unit cell of a crystal. We would like to point out that there are alternative ways of studying chemically disordered materials, like for example using the supercell approach. But in this study, we would like to reveal continuous crossovers on the phase diagram from one ground state to another, which would map the big picture of the chemical trends. The supercell approach would be prohibitively expensive for such studies, but can help in refining of the details. Besides, a mesh of different compositions (density of points), which have to cover the whole area of the ternary diagram of Ni-Mn-Ga would depend drastically on the size of the supercell. Evidently, by using the supercell approach the energy calculations will take more computational efforts as compared with the CPA. Therefore, in this work we focused on the CPA technique in spite of the fact that it is a mean field method. While it averages results and misses the important local chemical properties (including local symmetry), we still demonstrate that it helps to the "big" picture of the compositional dependence, which may stimulate more precise studies of particular areas on the ternary diagrams.

The maximum number of CPA iterations and the energy convergence tolerance were set to 20 and 0.01 mRy, respectively. For SCF cycles, the scattering path operator was calculated with the special method using a regular **k**-mesh grid of 57^3 with 4495 **k** points, and the BROYDEN2 scheme [18] was used with the exchange-correlation potential of PBE. For the SCF calculations the arc-like contour path in the complex energy plane has been chosen as in approach of weakly bound states which were treated as core states. The upper end of the energy path E_{max} was set to the Fermi energy E_F. For the real part of lowest energy value we have used the value of $E_{min} = -0.1$ Ry. The number of E-mesh points was set to 30. In order to achieve a faster convergence, the SCF mixing parameter was set to 0.20. The maximum number of SCF iterations was taken to 200.

Figure 2 shows the compositions of Ni-Mn-Ga that we used in this study, a mesh of forty equal spaced points. It is worth noting that in order to form off-stoichiometric compositions we fixed Ni, Mn, and Ga atoms at specific Wyckoff positions 8*c*, 4*a*, and 4*b*, respectively, according to the $Fm\underline{3}m$ space group. For example, in the case of $Ni_{0.6}Mn_{0.2}Ga_{0.2}$ ($Ni_{2.4}Mn_{0.8}Ga_{0.8}$) the atoms occupied the following positions: 8*c* [Ni, Ni], 4*a* [Mn(0.8), Ni(0.2)] and 4*b* [Ga(0.8), Ni(0.2)].

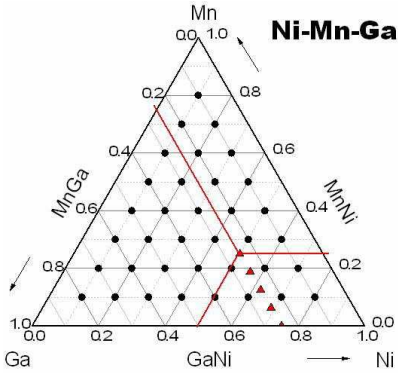

Figure 2. Ternary phase diagram of Ni-Mn-Ga. Here, the symbols show the compositions using in our calculations. The intersection point of three lines denotes the stoichiometric Ni_2MnGa alloy. Triangle symbols indicate the commonly studied set of $Ni_{2+x}Mn_{1-x}Ga$ compositions.

One of the biggest challenges in this work is to describe correctly various magnetic configurations that emerge due to the compositional mixing. Because of the fact that excess Mn atoms readily occupy the sites of 4*c* sites of Ni as well as the 4*b* sites of Ga, they can interact antiferromagnetically (AFM) with the Mn atoms sitting at their regular 4*a* sites. With a variety of magnetic configurations that may exist for each point on the ternary diagram, it is necessary to perform multiple calculations with different initial spin configurations. We limit our study to three spin configurations refereed as FM (spins of Mn located at the Ni, Mn, and Ga sites are parallel) and two ferrimagnetic ones: FIM-1 (spins of Mn located at the Mn and Ga sites are parallel while the spin of Mn at the Ni site is reversed) and FIM-2 (spins of Mn located at the Mn and Ni sites are parallel while the spin of Mn at the Ga site is reversed).

3 Results of *ab initio* calculations

First, in order to test the accuracy of the CPA calculations, we compared our lattice relaxations

obtained using the SPR-KKR package with a set of calculations obtained for the popular series of $Ni_{2+x}Mn_{1-x}Ga$ (x = 0, 0.25, 0.5, 0.75, and 1) alloys by means of the Quantum Espresso (QE) package [19]. Note the GGA-PBE approximation for the exchange-correlation functional as well as the 16 atoms-cell were used in these calculations. The comparison between the results obtained by the SPR-KKR and QE packages is shown in Fig. 3.

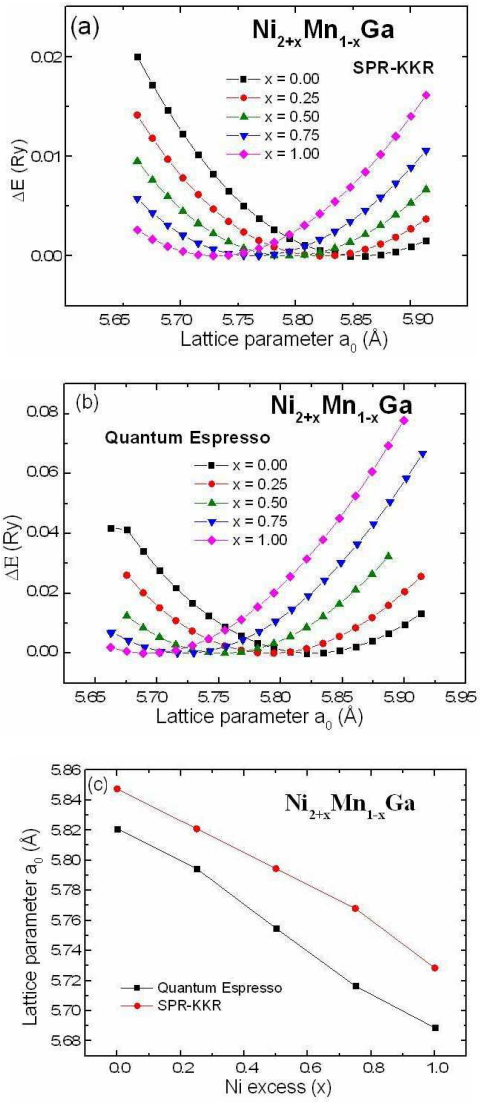

Figure 3. Total energy differences of $Ni_{2+x}Mn_{1-x}Ga$ as functions of the lattice parameter obtained by using the (a) SPR-KKR and (b) QE packages. (c) Equilibrium lattice constants of $Ni_{2+x}Mn_{1-x}Ga$ as a function of the excess of Ni.

We can see from Fig. 3 a similar behavior of the energy curves, namely, a decrease in the lattice parameter occurs with increasing Ni content. It is also seen that the values of the equilibrium lattice parameter for all compositions obtained by the SPR-KKR package are slightly larger (by ~ 0.3 Å) than the lattice parameters calculated using the QE package, which is expected due to the different approximations implemented in the two codes. But overall we see a good agreement and should expect our SPR-KKR calculations to produce meaningful results in the entire range of the ternary diagram. It should be noted that our theoretical values of the lattice parameter for Ni_2MnGa are close to the experimental 5.825 Å [2].

We saw in previous studies that exploration of new materials can be significantly facilitated by the high – throughput techniques, which provide a complete picture of the compositional dependence [20]. We adopt the same approach in this work, but using the theoretical methodology. Figure 4 shows an example of our data, which in this case is the equilibrium lattice parameter of the cubic austenite mapped on the ternary Ni-Mn-Ga diagram.

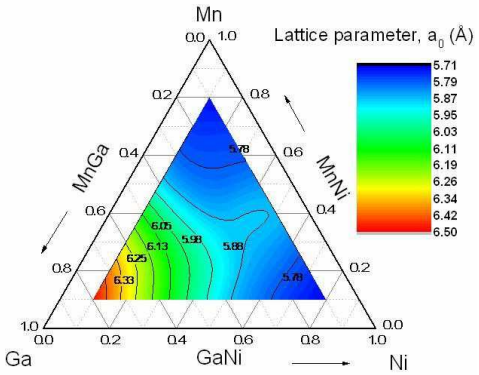

Figure 4. The distribution of the equilibrium lattice parameter mapped on the ternary diagram of Ni-Mn-Ga.

As one can see from Fig. 4, the largest lattice parameter (~ 6.4 Å) is observed at the bottom - left corner of the ternary diagram, indicating the compositions with the higher Ga content. Contrary to that, a decrease in the lattice parameter is found with increasing Ni and Mn contents. Correspondingly, areas with the minimal lattice parameter (~ 5.7 Å) located at the top and right corners of the diagram correspond to compositions with higher Mn and Ni concentrations, respectively. The larger lattice parameters for compounds with the excess of Ga is caused by the greater atomic radius of Ga as compared to Mn and Ni atoms while the atomic radii of the latter atoms are approximately equal to each other.

The distribution of the bulk modulus on the ternary diagram of Ni-Mn-Ga is shown in Fig. 5.

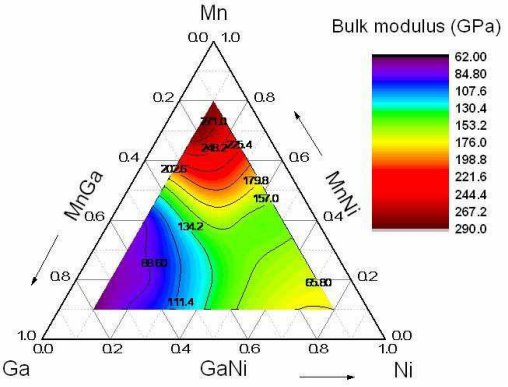

Figure 5. The distribution of the bulk modulus mapped on the ternary diagram of Ni-Mn-Ga.

It is found that the compounds with Ga excess (see the left corner of the diagram) have the lowest values for the bulk modulus (~ 72 GPa) whereas the mean values (~170 GPa) are observed for the compositions with Ni excess. Finally, the highest values (~ 265 GPa) are found for the alloys containing higher concentrations of Mn. The calculated value for the bulk modulus of the stoichiometric Ni_2MnGa alloy is close to 152 GPa and correlates well with the experimental value (148 GPa) [2]. The bulk modulus was calculated from the second-order derivative of the total energy (E), by using the following thermodynamic equation.

$$B = -V\left(\frac{\partial P}{\partial V}\right) = V\left(\frac{\partial^2 E}{\partial V^2}\right). \quad (1)$$

Here V_0 is the equilibrium volume, P and V are the external pressure and the cell volume, respectively.

In Fig. 6(a) we illustrate the mapping of the total magnetic moment on the ternary diagram of Ni-Mn-Ga. From this distribution it can be seen that the highest magnetic moment is observed for alloys with about equal concentrations of Ni and Mn, but no Ga. At the same time, areas with the smallest values of a magnetization are observed for the compositions with the Mn and Ga excess atoms. The ternary magnetic phase diagram in Fig. 6(b) shows the regions with stable magnetically ordered FM and FIM-1 phases.

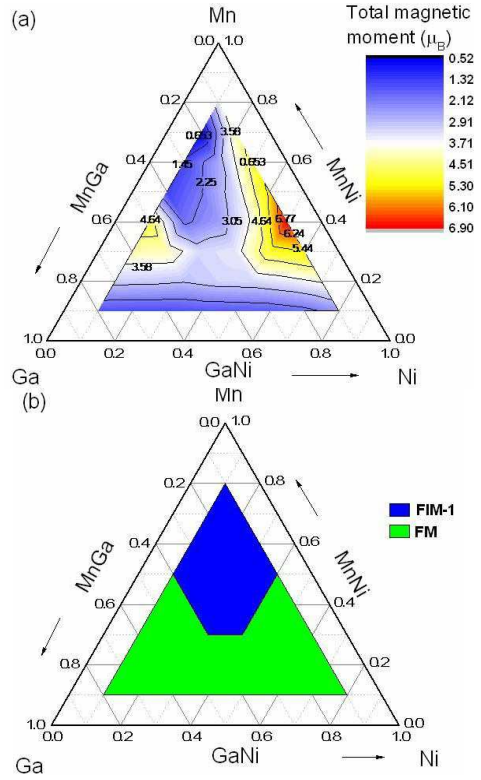

Figure 6. (a) The distribution of the total magnetic moment mapped on the ternary diagram of Ni-Mn-Ga. (b) Magnetic ternary phase diagram of Ni-Mn-Ga.

Our calculations show that the FIM-2 spin configuration is not favourable in any of the compositions of the cubic $L2_1$ austenite. We can also observe that the FM alignment is more stable in about two thirds of the compositions, whereas the stable FIM-1 configuration is more stable in compositions with higher Mn content. It should be noted that the average value of the magnetization in the FIM-1 phase is almost the same as in the lower part of FM phase (See Fig. 6(a)). This is due to the fact that the compounds located in the lower part of the ternary diagram have a large concentration of Ga atoms possessing negligibly small magnetic moments.

In order to investigate the phase stability of the off-stoichiometric Ni-Mn-Ga compositions with different magnetic configurations, we calculate their formation energies for the cubic phase. It should be noted that the formation energy is defined as a difference between the total energy of the alloy and the concentration weighted average of the pure atomic species, as follows:

$$\Delta E_{mix} = E_{tot} - \left(xE^{Ni} + yE^{Mn} + zE^{Ga}\right), \quad (2)$$

where, E_{tot} is the total energy of alloy, x, y, z are the concentrations of Ni, Mn, and Ga atoms, $E^{Ni(Mn,Ga)}$ are the pure element total energy of Ni, Mn, and Ga atoms, respectively. The negative value of formation energy indicates the phase stability.

The formation energies for the cubic lattice of Ni-Mn-Ga alloys mapped on the ternary diagram are shown in Fig. 7.

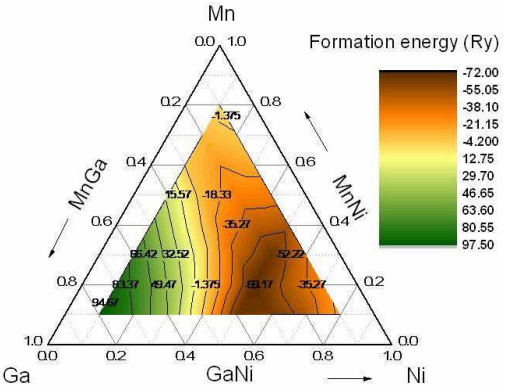

Figure 7. The distribution of the formation energy mapped on the ternary diagram of Ni-Mn-Ga.

It is evident from the figure that the formation energies for the compounds with Ni and Mn excesses atoms have negative values while for alloys with a high Ga content the positive values of the formation energies indicate that those structures are unstable. It is important to note that the most stable compositions are found in the same range, which is shown in Fig. 1 as the most actively explored experimentally. Now, from the theoretical perspective we can see that the experimentally studied area on the ternary diagram of Ni-Mn-Ga is directly related to the energetics of those structures. However, we see from our data that expanding the experimentally area shown in Fig. 1 straight down towards the $Ni_{0.57}Mn_{0.1}Ga_{0.33}$ composition can be rather promising, because our calculations show that region to be even more stable than the stoichiometric Ni_2MnGa.

4 Conclusions

A systematic study of the magnetic and structural properties of Ni-Mn-Ga alloys has been performed by means of *ab initio* calculations. The results of our calculations allow to map equilibrium lattice parameters, total magnetic moments, the bulk moduli, and the formation energies on the entire spread of the compositional ternary diagram of Ni-Mn-Ga. We have shown that the area of compositions with a higher Ga content has the largest lattice parameter and the smallest bulk modulus, but those compositions are chemically unstable. On the other hand, the area with the higher Ni content has the smallest lattice parameter, exhibits the FM ordering and about average values of the bulk modulus. Finally, the largest bulk moduli and the smallest lattice parameters were found in compositions with the higher Mn content, but those compositions tend to become ferrimagnetic. Calculations of the formation energies show that compositions in the area around the stoichiometric alloy Ni_2MnGa are the most stable, which explains why exactly this range has been covered so far in the experimental studies reported in the literature.

Acknowledgments

This work was supported by RFBR Grant No. 14-02-01085, RSF No. 14-12-00570\14 (Section 2), Ministry of Education and Science of Russian Federation (RF) No 3.2021.2014/K (Section 3), and CRDF Grant No. FSCX-15-61151-0. ATZ thanks for the computational resources from OSC (PCS0220) and XSEDE (TG-DMR130080).

References

1. P. J. Webster, J. Phys. Chem. Solids **32**, 1221 (1971)
2. P. J. Webster, K. R. A. Ziebeck, S. L. Town et al. Phil. Mag. B **49**, 295 (1984)
3. K. Ullakko, J. K. Huang, C. Kantner et al. Appl. Phys. Lett. **69**, 1966 (1996)
4. A.N. Vasil'ev, A.D. Bozhko, V.V. Khovailo et al. Phys. Rev. B **59**, 1113 (1999)
5. A. N. Vasiliev, V. D. Buchelnikov, T. Takagi et al. Physics-Uspekhi **46**, 559 (2003)
6. C. Jiang, Y. Muhammad, L.Deng et al. Acta Mater. **52**, 2779 (2004)
7. N. Lanska, O. Soderberg, A. Sozinov et al. J. Appl. Phys. **95**, 8074 (2004)
8. V.V. Khovailo, V.D. Buchelnikov, R. Kainuma et al. Phys. Rev. B **72**, 224408 (2005)
9. M. Richard, J. Feuchtwanger, D. Schlagel et al. Scripta Mater. **54**, 1797 (2006)
10. P. Entel, V.D. Buchelnikov, V.V. Khovailo et al. J. Phys. D: Appl. Phys. **39**, 865 (2006)
11. A.T. Zayak, W.A. Adeagbo, P. Entel, K.M. Rabe, Appl. Phys. Lett. **88**, 111903 (2006)
12. V.D. Buchelnikov, V.V. Sokolovskiy, H.C. Herper et al. Phys. Rev. B **81**, 094411 (2010)
13. C.-M. Li, H.-B. Luo, Q.-M. Hu et al. Phys. Rev. B **84**, 174117 (2011)
14. A. Cakr, L. Righi, F. Albertini et al. J. Appl. Phys. **114**, 183912 (2013)
15. X. Xu, M. Nagasako, W. Ito et al. Acta Mater. **61**, 6712 (2013)
16. H. Ebert, D. Ködderitzsch, and J. Minár, Rep. Prog. Phys. **74**, 096501 (2011)
17. P. Perdew, K. Burke, M. Enzerhof, Phys. Rev. Lett. **77**, 3865 (1996)
18. C.G. Broyden, Math. Comp. **19**, 577 (1965)A. Planes, Ll. Manosa, M. Acet, J. Phys. Condens. Matter **21**, 233201 (2009)
19. Quantum ESPRESSO package Version 5.02 at http://www.pwscf.org
20. I. Takeuchi, O.O. Famodu, J.C. Read et al. Nature Materials **2**, 180 (2003)